

Evaluation of a ramjet model in a supersonic high-enthalpy tunnel

*G. Riva, * and G. Daminelli **

** Consiglio Nazionale delle Ricerche, CNR-ICMATE, Via Cozzi, Milano
53 Via Cozzi, Milano, Italy*

*C. Paravan **, F. Maggi **, G. Colombo **, A. Verga **, R. Bisin **, S. Carlotti **, L. Galfetti ***

*** Politecnico di Milano, Department of Aerospace Science and Technology
Space Propulsion Laboratory (SPLab)*

34 Via La Masa, 20156, Milan, Italy – luciano.galfetti@polimi.it

Abstract

In the framework of a cooperation agreement between SPLab of Politecnico di Milano and ICMATE-CNR (National Research Council), two different configurations of a rectangular geometry small scale model engine fuelled with gaseous hydrogen were tested at Mach 5.4 in a high enthalpy pulse facility. A dual-mode scramjet setup was first studied and the main propulsion parameters were obtained for a wide ER range. A second geometry, corresponding to a ramjet configuration, was then evaluated under the same nominal freestream flow and fuelling conditions. Under the tested flight conditions, the ramjet setup featured higher specific impulses.

1. Introduction

The unclassified research activity and progresses in high-speed flight during the past decades are described in several contributions in which extensive references are given, for example the fine overview by Northam and Anderson [1], or by Curran [2], among the others. General reviews of research activities and flight-demonstrated technology have also been presented [3]. In recent years hypersonic prototypes were successfully operated in flight for a few seconds at Mach 7 and 10 [4] and for about 200 s at Mach 5 [5]. Tests covering the flight speed of concern were carried out in the high-enthalpy pulse facility of CNR (the Italian National Research Council, ICMATE Institute, in Milano), used in the past for studies on scramjet inlets at hypersonic speed.

Combined cycle propulsion systems may be a convenient option for space launchers because of their capability to take advantage of the atmospheric oxygen during the ascent trajectory. In particular, high-supersonic and hypersonic flight regimes can be covered by ramjet and scramjet operation modes [6]. In order to cover a flight Mach number range as wide as possible without geometry changes, the concept of dual-mode combustion has been proposed [7]. In these systems, ramjet mode can be made to occur in a scramjet geometry by producing a thermal choking that replaces the physical throat at the combustion chamber exhaust [8]. The transition between subsonic and supersonic combustion modes is usually set in the flight Mach number range from 5 to 8. Curran and Stull [7], for example, consider Mach 8 as the lower limit for scramjet operation; Kanda et al., [9], place the transition at Mach 7; Siebenhaar et al. [10] consider, for the Strutjet Rocket-Based Engine, an upper limit for ramjet mode at Mach 6.3; Waltrup et al. [11] report diagrams showing that, above Mach 6, scramjet becomes superior to ramjet in terms of specific impulse, with either hydrogen or borane as fuel. The amount of fuel injected and burned also affects the combustion mode: Rockwell et al. [12], for example, in experimental studies on the effect of air vitiation on combustor performance, while working with enthalpies simulating Mach 5 flight conditions, found supersonic combustion for equivalence ratios below 0.22, and subsonic combustion above 0.26 with clean air, but observed that air flow vitiation increases the equivalence ratio (ER) at which transition occurs. Turner and Smart [13] studied the combustion mode change at Mach 8 in a scramjet model. Two combustion chamber configurations characterized by the same total length and area ratio, but different lengths of the constant area section were tested for equivalence ratio in the range 0-2. For longer constant area section, transition

from supersonic to “separated” combustion occurred at $ER = 0.91-0.98$ and produced an abrupt thrust and combustion efficiency increments, whereas the short constant area section setup featured a smoother transition at $ER = 1.33-1.62$.

In the present work, two different configurations of a rectangular geometry small scale model engine were tested at Mach 5.4 in a high enthalpy pulse facility used in the past for studies on hypersonic (Mach 8) inlets [14] and tests on a ramjet model at Mach 4.5 [15]. The adoption of rectangular geometry allows easy change of the shape of the engine internal channels by simple translation of the side walls, while maintaining constant height. This “parametric” engine concept has been adopted in the past [16], and turned out to be useful when operation mode transitions requiring different geometry setup are of concern, or when investigating on the performance of engine components such as inlets or nozzles. For example, in [15], the throat area of a ramjet exhaust nozzle was parametrically changed in non-fuelled tests in order to test the limit combustion chamber pressure before inlet unstart. A typical ramjet setup comprising inlet, step combustor, and convergent divergent nozzle was first tested for a wide range of fuelling conditions. The convergent part of the nozzle was then removed, to obtain a geometry with constant area combustion chamber, followed by a divergent nozzle, typical of dual-mode scramjets. This setup was tested under similar flight and fuelling conditions and the propulsion parameters compared with those obtained for the ramjet geometry.

All tests were carried out in the high-enthalpy pulse tunnel of the Consiglio Nazionale delle Ricerche – Istituto di Chimica della Materia Condensata e di Tecnologie per l’Energia (CNR-ICMATE) [15, 17]. The facility can simulate flight conditions in the Mach number range from 3 to 8, with dynamic pressures within the field usually considered for airbreathing hypersonic propulsion [18]. In this case, the freestream Mach number was about 5.5, and the dynamic pressure approximately 40 kPa. The required total enthalpy level was obtained by hydrogen pre-combustion in a 70 liters volume vessel. As a consequence, the freestream test flow was vitiated by 20% water vapour in volume, while preserving 21% of oxygen volume fraction. Test times of about 200 ms are usually obtained, in which the model engines can operate with started inlet and produce thrust. Within this time window, the freestream pressure and temperature decay is relatively slow if compared with the flow residence time inside the model engine, thus allowing the analysis of the acquired data according with the quasi-steady assumption.

2. Small scale parametric engine

A dual-mode scramjet configuration (SCRAM) was first tested, whose geometry is given in Fig. 1, where a schematic view of bottom surface and shape of the side walls is shown, with the top plate ideally removed.

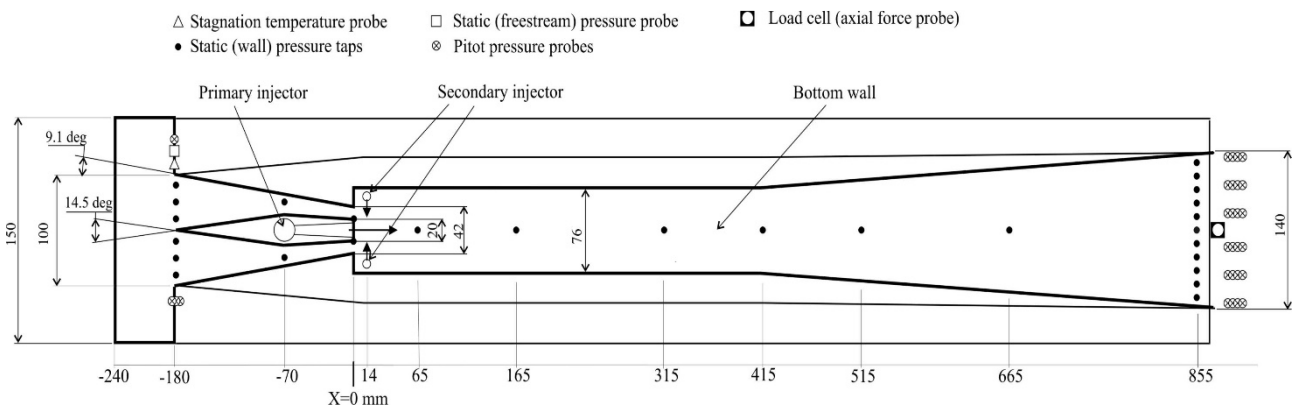


Figure 1: Top view schematic of the dual mode scramjet setup (SCRAM), showing side walls configuration, components of the staged injection system, and location of pressure, temperature, and force sensors.

The engine intake and exhaust are, respectively, 100 and 140 mm wide. The height is 40 mm, constant along the entire engine, whose total length is 1100 mm. The bottom surface includes a flat plate with sharp leading edge, 60 mm length, 150 mm width, upstream of the engine intake section. The inlet internal geometry includes sidewall compressor and an internal strut that splits the captured air flow in two identical streams. The central strut embodies a small gas fuelled rocket engine that may be used either as a torch to start combustion into the main engine combustion chamber, or as a primary fuel injector (Fig. 2). When used ignition torch, a spark plug is used to start combustion inside the rocket, usually fed with gaseous $H_2 - O_2$. Fuel or combustion product are injected into the engine combustor from the strut back face through three diverging channels. Most of the compression of the captured air flow is performed into the first part of the inlet, whereas the second part features a modest compression ratio and contributes to isolate the inlet from the backpressure generated inside the combustion chamber during the engine operation. The overall geometric

contraction ratio is 0.22. A step combustor consisting of a constant area channel, 410 mm length, 76 mm width follows the compressor. The exhaust nozzle is a 450 mm length channel, with 8 deg total angle diverging sidewalls. The exhaust section is 40 mm height and 140 mm width. Aluminium was used for the model support and engine structure, whereas stainless steel was adopted for the internal walls.

A staged fuel injection system is present at the combustor inlet. In addition to the primary system embodied into the central strut, a secondary injector consisting of two vertical pipes, 6 mm external diameter, 40 mm length, is present (Fig. 2). The pipes, each carrying 6 holes, 1,1 mm diameter and oriented normally with respect to the main flow direction, are placed symmetrically with respect to the engine vertical mid-plane, inside the recirculation regions behind the backward facing step of the combustor inlet section. The secondary injection operation is totally separated from the primary injection system, as it takes fuel from a separate reservoir, and feeds the engine through an independently operated solenoid valve. As shown in Fig 1, the staged injection system performs both parallel (primary) and normal (secondary) injection with respect to the main flow direction, thus generating four main fuel-air interface regions.

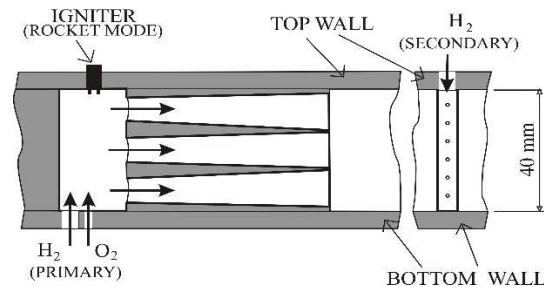


Figure 2: Partial cross-sections on the vertical engine mid-plane, showing details of the staged fuel injection system. The primary injector may also be operated as ignition torch or rocket, whereas the secondary injector feeds room temperature gaseous fuel.

A staged fuel injection system is present at the combustor inlet. In addition to the primary system embodied into the central strut, a secondary injector consisting of two vertical pipes, 6 mm external diameter, 40 mm length, is present (Fig. 2). The pipes, each carrying 6 holes, 1,1 mm diameter and oriented normally with respect to the main flow direction, are placed symmetrically with respect to the engine vertical mid-plane, inside the recirculation regions behind the backward facing step of the combustor inlet section. The secondary injection operation is totally separated from the primary injection system, as it takes fuel from a separate reservoir, and feeds the engine through an independently operated solenoid valve. As shown in Fig 1, the staged injection system performs both parallel (primary) and normal (secondary) injection with respect to the main flow direction, thus generating four main fuel-air interface regions.

A further setup of the parametric engine was tested (Fig. 3). The relevant geometry change is a throat placed at the end of the constant area channel that shrinks the channel width from 76 to 61 mm. The inlet section is also slightly modified as the side walls compression angle is reduced from 9.1 to 8.9 deg., with a consequent modification of the overall geometric contraction ratio from 0.22 to 0.24. The resulting configuration is a ramjet engine setup whose components are inlet compressor, a 360 mm length, constant section, step combustion chamber, and a convergent divergent nozzle. All other components of the engine, including staged fuel injection system and location of the pressure, temperature and force probe locations, are identical for the two configurations.

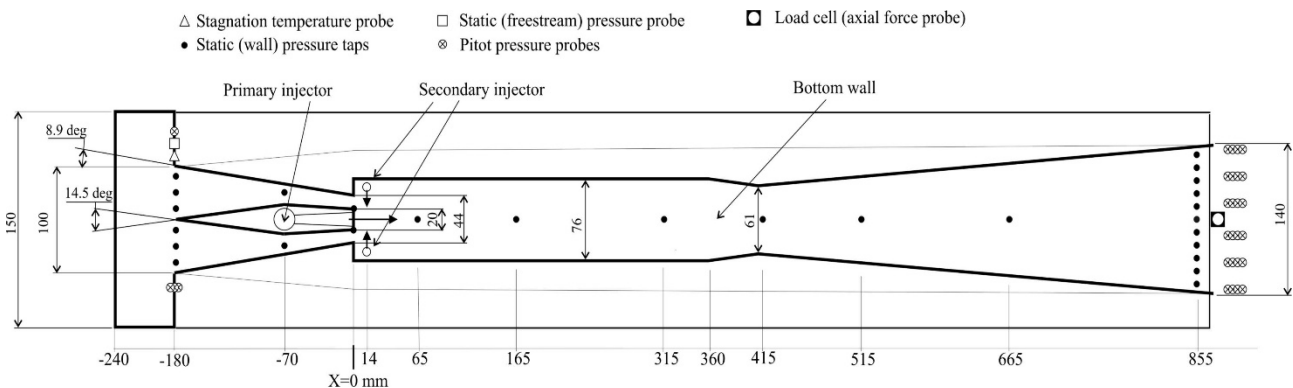


Figure 3: Top view schematic of the ramjet setup (RAM), showing side walls configuration, components of the staged injection system, and location of pressure, temperature, and force sensors.

3. Diagnostics and data acquisition system

Each test is characterized by freestream static and pitot pressures and stagnation temperature measurements (Figs. 1, 3). These quantities are detected in the unperturbed facility nozzle flow near the engine capture area and allow the evaluation of freestream Mach number, dynamic pressure, and static temperature during the entire test time. A set of three pitot probes placed near the external engine sidewall on one side of the intake section is used to characterize the flow pattern produced by the bottom plate leading edge (Fig. 4). It was observed, in fact, that the sharp leading edge produces an oblique shock wave swallowed by the inlet during normal engine operation with started inlet.

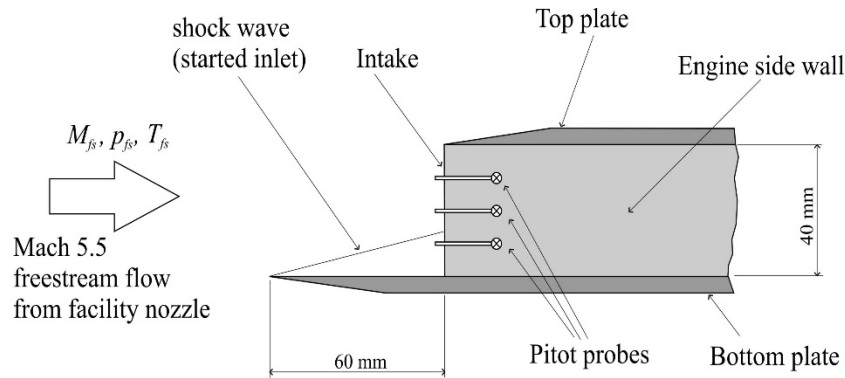


Figure 4: Schematic side view of the engine inlet, showing the pitot probes placed at 10, 20, and 30 mm above the bottom surface, used to characterize the airstream captured by the engine.

Static (wall) pressure on the bottom plate is measured by six ports in the inlet section and inside the engine compressor, combustion chamber, and nozzle on the locations shown in Figs. 1 and 3. The engine exhaust flow is characterized in detail by eleven wall pressure ports on the bottom wall that and a 24 pitot probes array covering the entire exhaust section (Fig. 5).

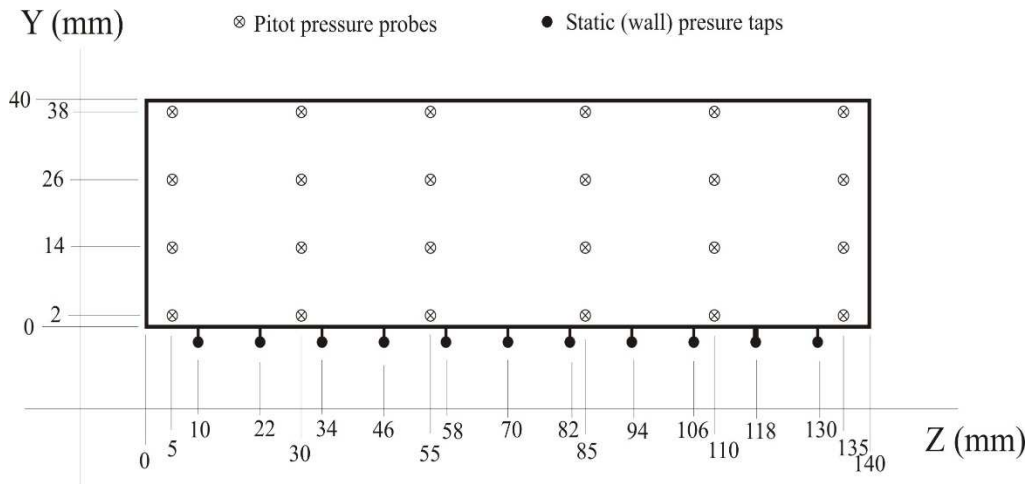


Figure 5: Static and pitot pressure monitoring locations map on the engine exhaust section.

Axial forces experienced by the engine and its support structure are detected by a 5000 N full scale load cell, whose total error is less than $\pm 0.03\%$ of the load. Pressure measurements are performed with piezoresistive transducers of appropriate full scale range, 100kHz (or higher) natural frequency and 1% (or less) global accuracy. The freestream stagnation temperature is evaluated by a homemade probe based on the electrical resistance change with temperature of a 80 micron diameter iridium wire.

4. Test procedure and data analysis

All tests were conducted at Mach 5.4 with vitiated air obtained from the hydrogen pre-combustion. As a first step, the stagnation reservoir of the facility is filled with a mixture of air, oxygen and hydrogen. The pre-combustion is started by means of a multiple system of spark plugs to improve the repeatability and minimize the combustion time. The combustion products include 20% water vapor and 21% oxygen volume fractions. After a pre-selected time interval the vessel is connected to the facility nozzle through a pressure driven valve, producing the test flow at the nominal flight Mach number. The flow stabilization inside the engine is monitored by the internal pressure time histories that, when normalized using the freestream pressure, always become approximately constant in time within a few milliseconds, indicating a quasi-steady behavior with respect to the external flow conditions. After the flow stabilization in the model, the fuel is fed from primary and/or secondary injectors into the engine combustion chamber. The primary injector (Figs. 1, 2, 3) is initially fed with both hydrogen and oxygen and operated in rocket mode for approximately 40 ms, thus acting as ignition torch of the ramjet combustion chamber. The rocket mode operation is terminated by shutting the oxygen valve, while the primary hydrogen injection can either be maintained or removed. Self sustained combustion in the ramjet combustion chamber is normally maintained after switching to pure fuel injection.

The data base from each experimental test is analyzed in order to obtain the time histories of parameters such as thrust, specific impulse, specific thrust, equivalence ratio, combustion efficiency. A complete analysis of the engines performance is carried out with 0.5 ms time step for the relevant portion of the test time, that is from the start of the test flow to the facility nozzle unstart. Averages were also computed over a 90 ms time interval characterized by a freestream average static temperature in the range 210-220 K. The averaging procedure gives a static pressure of about 2000 Pa, corresponding to an altitude of about 26.5 km, and a dynamic pressure of 40 kPa on the same interval, with total variations in time associated with the nature of the pulse facility flow of about $\pm 20\%$ for static and dynamic pressure, and $\pm 10\%$ for the static temperature. The relatively large variation of static pressure, dynamic pressure, and static temperature are a consequence of the wide averaging time window. The correct operation mode over the entire window demonstrates that combustion and thrust generation are well established and stable conditions of the engine. The freestream Mach number change is confined within $\pm 1\%$ of the average value. The averaging interval starts about 25 ms after the end of the rocket operation mode of the primary injector, that is when pure fuel is fed into the ramjet model and self sustained combustion is achieved.

5. Results: time dependent representation

Each test provides a database that comprises the time evolution of pressure, temperature and axial force detected by the sensors schematically shown in Fig. 1 or Fig. 3. Further measurements provide the hydrogen and oxygen injection pressure for staged fuel injection system. The large number of tests carried out under different fuelling conditions requires a synthetic representation of each measured and computed parameter. A time window is thus defined for each test in such a way as to characterize the quasi steady working regime of the engine for freestream pressure, temperature, and Mach number that better simulate the real flight conditions.

The wall pressures at several monitoring locations on the engine bottom wall are given in Fig. 6. The engine inlet pressure ($x=-180$ mm in Fig. 1) is monitored by 6 probes that cover the entire intake width. All probes measure nearly identical pressure levels, thus indicating a uniform pressure field in the spanwise direction. The pressure measured by the probe at $x=165$ mm, inside the constant area channel, shows clearly the effect of the combustion process lasting approximately 200 ms. The engine exhaust pressure is monitored at 11 equally spaced locations along the spanwise direction. The nearly coincident traces indicate uniform pressure during the entire combustion transient.

The freestream and engine exhaust total temperatures are given in Fig. 7. The plot comprises the temperature of the iridium wire that provides the database for the evaluation of the freestream total temperature, obtained taking into account wire thermal inertia, and energy lost from the wire ends and by radiation. The engine exhaust temperature is obtained from mass conservation equation and detailed measurements of exhaust static and pitot pressures, being the gas thermo-physical properties provided by the energy conservation equation.

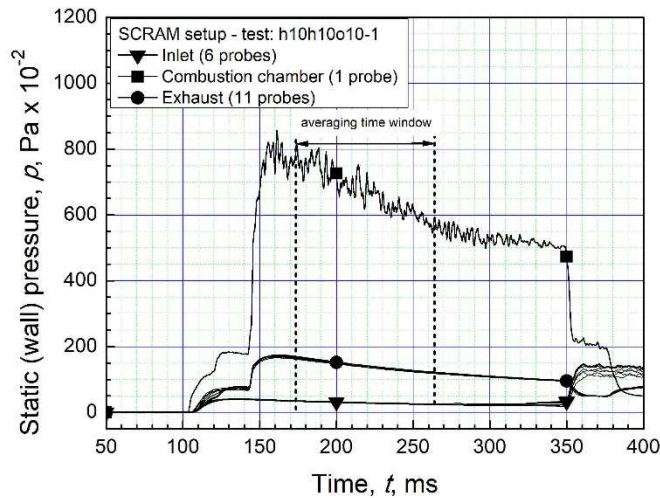


Figure 6: Wall pressure traces detected at engine inlet, centre of combustion chamber, and engine exhaust for a fuelled case, and SCRAM geometry setup. The averaging time interval is also indicated.

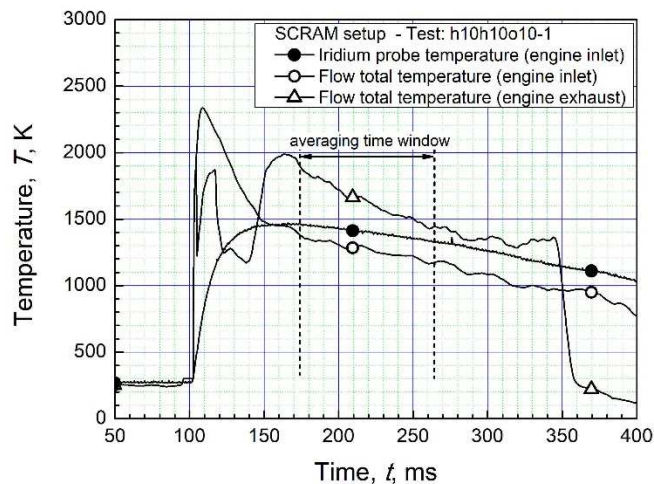


Figure 7: Iridium probe temperature, freestream total temperature obtained from probe data, and engine exhaust total temperature, obtained from pressure measurements and conservation equations.

Engine fuelling is implemented in such a way as to keep ER nearly constant during the test time, as shown in Fig. 8. This condition is obtained with appropriate sizes of fuel reservoirs and injection portholes that provide a discharge law consistent with the one of the facility stagnation vessel producing the freestream flow. The combustion efficiency, evaluated from energy conservation equation, features a slow decrement during the combustion time, as both freestream pressure and temperature decrease, but also indicates that the engine may withstand changes of the flight conditions without excessive performance penalties.

Pressure measurements on the engine bottom wall combined with conservation equations allow the estimation of the bulk flow Mach number at pressure monitoring locations inside the engine. Because of the complex structure of the internal flow and the fact that pressure at some monitoring locations may not be representative of the average on the corresponding engine section, the Mach numbers obtained are only indicative, but may at least provide information about the subsonic or supersonic nature of the flow. The Mach numbers reported in Fig. 9 refer to six axial locations including freestream flow, end compressor, constant area channel, engine exhaust. When multiple wall pressure taps are present on a section, the average value was considered. As combustion starts (140 ms, Mach numbers inside the engine significantly decrease and, in particular, in the constant area combustion chamber becomes subsonic. The three monitoring locations along the constant area channel indicate an increasing velocity flow that reaches sonic conditions

before the start of the diverging channel, thus producing a “thermal throat”. The flow accelerates into the downstream diverging channel, whose exhaust is supersonic. The Mach numbers remain constant during the whole combustion time. A similar analysis on non fuelled tests shows the flow is fully supersonic along the entire engine and for both SCRAM and RAM geometry configurations.

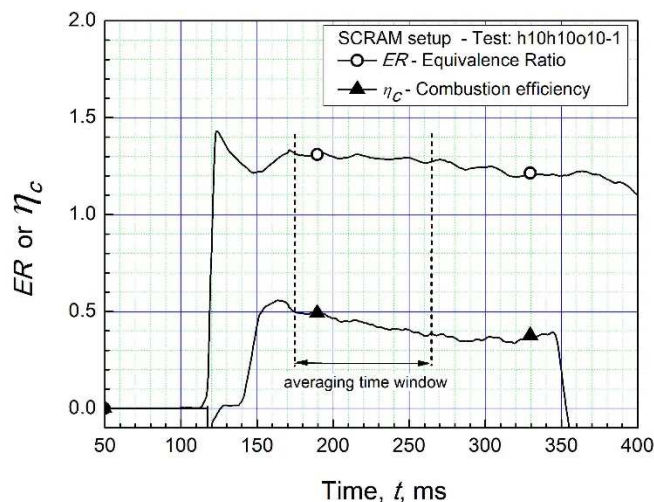


Figure 8: Equivalence ratio and combustion efficiency as function of time. Equivalence ratio is nearly constant, whereas combustion efficiency slowly decrease, but indicates a stable and self sustained combustion lasting approximately 200 milliseconds.

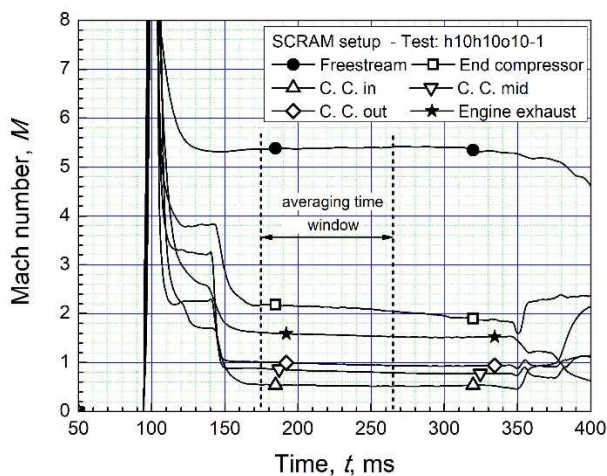


Figure 9: Freestream and internal engine Mach numbers at different locations including end compressor, constant area combustion chamber, and exhaust section.

The time dependent uninstalled thrust is given in Fig. 10. It must be noticed that, as the freestream flow starts, the axial force becomes negative (engine drag). Fuel injection and combustion produce positive thrust lasting about 200 ms, whose trend replicates and amplifies the behaviour of the combustion efficiency. As done for all parameters, the averaging time window is centred on the time at which the freestream flow better approximate the real flight conditions.

Specific impulse and specific thrust are qualifying fundamental propulsion parameters, independent on the engine size. Fig. 11 shows that, according with their formulation, the trend replicates the behaviour of the uninstalled thrust. The values inside the averaging time window are relatively low because of the unfavourable condition of working in a pulse facility with vitiated freestream flow, cold internal walls and small size model, that maximize the energy losses.

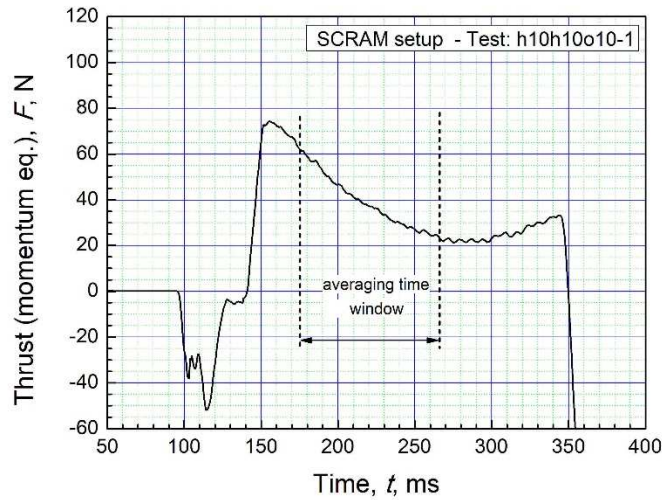


Figure 10: Engine uninstalled thrust evaluated from momentum equation.

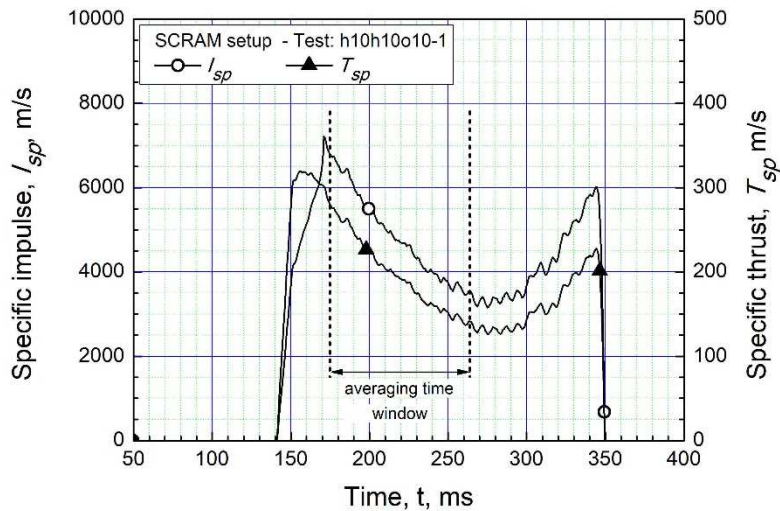


Figure 11: Specific impulse and specific thrust: only positive parts related to fuelled conditions are shown.

6. Results: time averaged representation

Combustion efficiencies are similar for the two geometries, as shown in Fig. 12. The data points distribution makes evident the different fuelling regimes required by the two engines, with the RAM upper boundary limited at ER 1.4 by inlet unstart, and the SCRAM lower boundary limited at ER=0.7 by the capability of sustain combustion.

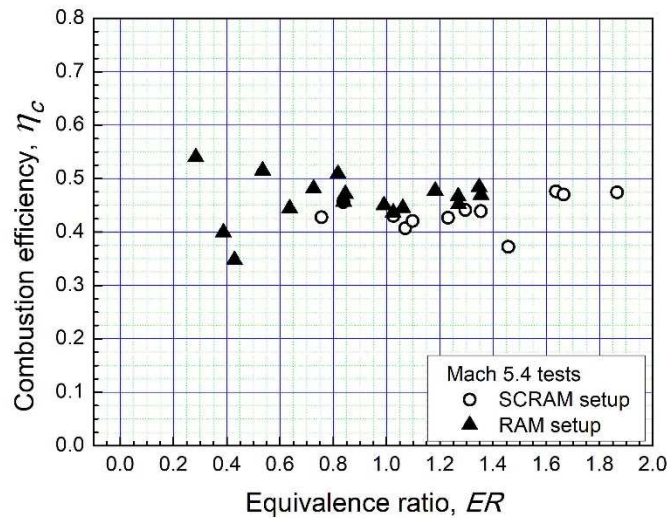


Figure 12: Combustion efficiencies for RAM and SCRAM geometries.

Both engines produced positive thrust, as shown in Fig. 13. The RAM setup featured self-sustained combustion starting from low ER. For $ER < 0.6$, however, combustion did not generate sufficient thrust to overcome the engine drag, estimated around 35 N for non-fuelled tests. For $ER > 0.6$ the engine produced positive thrust, with the maximum of 50-60 N at ER 1.3-1.4. All tests performed with higher fuel mass flow rates produced inlet unstart, with consequent sudden drop of thrust and all propulsion parameters. In the SCRAM setup, self-sustained combustion could not be obtained below $ER = 0.7$, at least with the combustion initiation technique adopted in all tests. Two tests inside the working fuelling range ($ER = 0.94$ and $ER = 1.41$) also featured unsuccessful ignition. Unlike for the RAM configuration, inlet unstart was never observed, even for the highest fuelling rates tested. A maximum net thrust of about 60 N was found for both geometries, but the highest value was reached at a higher fuelling rate ($ER = 1.9$) for the SCRAM setup. In the common working range, the RAM setup generates higher thrust for assigned ER. The direct consequence of this fact is that the RAM engine is characterized by a systematically higher specific impulse on the whole common working fuelling regimes. According with the results shown in Fig. 14, the best fuelling condition is around stoichiometry for the RAM geometry, whereas fuel-rich operation is the best option for the SCRAM setup.

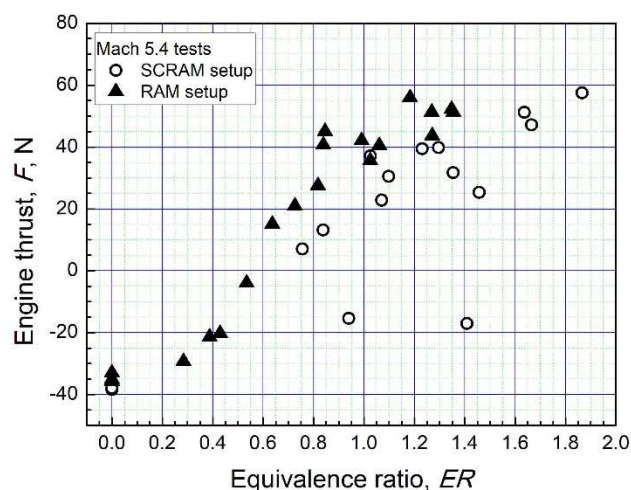


Figure 13: Uninstalled net thrust vs. fuelling regime for RAM and SCRAM geometries.

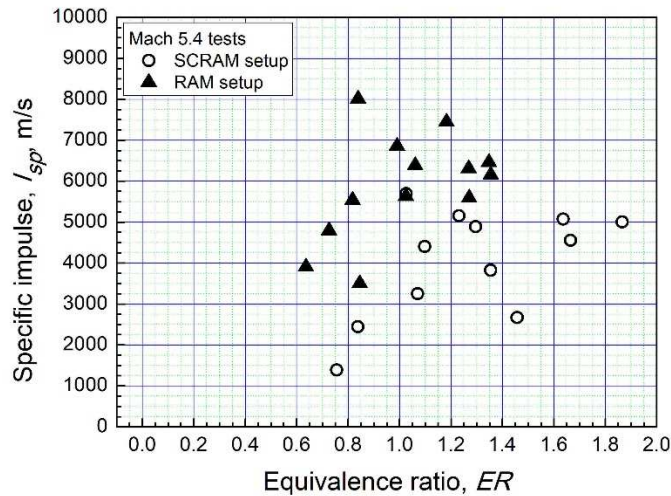


Figure 14: Specific impulse vs. fuelling regime for RAM and SCRAM geometries.

7. Conclusions

Both ramjet and dual-mode scramjet geometries demonstrated their capability to sustain stable combustion and generate positive thrust under Mach 5.4 simulated flight speed at 26.5 km altitude. Thrust generation was also maintained over a wide freestream flow pressure and temperature range centred on the nominal simulated flight conditions. The fuelling regimes required by the two engines were different. In particular, the RAM configuration sustained stable combustion on the ER range from 0.3 to 1.4, although positive thrust generation was observed only above 0.6, and being the upper limit imposed by inlet unstart. The RAM engine featured the highest specific impulse at nearly stoichiometric fuelling regimes. The SCRAM setup did not support self sustained combustion below $ER=0.7$, but never induced inlet unstart, at least, for the ER range investigated, whose upper limit was 1.9. The maximum thrust was nearly the same for the two engines, but was obtained at $ER=1.2$ with the RAM, and at $ER=1.9$ with the SCRAM geometry. Within the common fuelling regimes, the RAM setup systematically provided higher thrust and specific impulse. The 1D analysis of the engines internal flow, although based on a limited number of pressure monitoring locations, demonstrated that supersonic flow was maintained in all engine components during non fuelled tests for both RAM and SCRAM geometries. In all fuelled tests and in both engines, combustion induced subsonic flow inside the combustion chamber. In the SCRAM setup, thermal choking was found at the end of the constant area channel, where sonic conditions were always established. The tests performed indicate the RAM setup as the preferred option for the investigated flight regime as, in spite the nearly identical maximum thrust generated by the two engines, its specific impulse resulted systematically higher.

References

- [1] Northam, G.B., and Anderson, G.Y., "Supersonic Combustion Ramjet Research at Langley", 24th AIAA Aerospace Sciences meeting, AIAA Paper 1986-0159, Reno, NV, Jan. 1986.
- [2] Curran, E.T., "Scramjet Engines: The first Forty Years", *Journal of Propulsion and Power*, Vol. 17, N. 6, Nov-Dec 2001, pp. 1138-1148. doi: 10.2514/2.5875.
- [3] Fry, R.S., "A Century of Ramjet Propulsion Technology Evolution", *Journal of Propulsion and Power*, Vol. 20, N. 1, Jan.- Feb. 2004, pp.27-58. doi: 10.2514/1.9178.
- [4] Voland, R.T., Huebner, L.D., and McClinton, C.R., "X-43A Hypersonic Vehicle Technology Development", *Acta astronautica*, Vol. 59, Nos. 1-5, Jul.-Sep. 2006, pp. 181-191. Doi: 10.1016/j.actaastro.2006.02.021.
- [5] Hank, J.M., Mutphy, J.S., and Mutzman, R.C., "The -51A Scramjet Engine Flight Demonstration Program", 15th AIAA International Space Planes and Hypersonic Systems and Technologies Conference, AIAA Paper 2008-2540, Dayton, OH, May 2008.

-
- [6] Heiser, W.H., and Pratt, D.T., *Hypersonic Airbreathing Propulsion*, AIAA Education Series, edited by J.S. Przemieniecki, AIAA education Series, AIAA, Washington DC, 1994.
- [7] Curran, E.T., and Stull F.D., "The Utilization of Supersonic Combustion Ramjet Systems at Low Mach Numbers", AF Aero Propulsion Laboratory, RTD.TDR-63-4097, January 1964.
- [8] Heiser, W.H., and Pratt, D.T., "Aerothermodynamics of the Dual-Mode Combustion Systems", in *Scramjet Propulsion*, E.T. Curran, and S.N.B. Murthy Editots, Progress in Aeronautics and Astronautics, Vol. 189, 2000.
- [9] Kanda, T., Tani, K., and Kudo, K., "Conceptual Study of a Rocket-Ramjet Combined-Cycle Engine for an Aerospace Plane", *Journal of Propulsion and Power*, Vol.23, N. 2, March-April 2007.
- [10] Siebenhaar, A., Bulman,M.J., and Bonnar, D.K., "Strutjet Rocket-Based Combined-Cycle Engine", in *Scramjet Propulsion*, E.T. Curran, and S.N.B. Murthy Editors, Progress in Aeronautics and Astronautics, Vol. 189, 2000.
- [11] Waltrup, p.j., Anderson, G.Y., and Stull, F.D., "Supersonic Combustion Ramjet/Scramjet Engine Development In the United States", The 3rd International Symposium on Air Breathing Engines, Munich, Germany, 1976.
- [12] Rockwell, R.D., Goyne, C.P., Haw, W., Krauss, R.H., McDaniel, J.C., and Trefny, C.J., "Experimental Study of Test-Medium Vitiation Effects on Dual-Mode Scramjet Performance", *Journal of Propulsion and Power*, Vol.27, N.5, September-October 2011.
- [13] Turner, J.C., and Smart, M.K., "Mode Change Characteristics od a Three-Dimensional Scramjet at Mach 8", *Journal of Propulsion and Power*, Vol. 29, N. 4, July-August 2013.
- [14] Riva, G., Reggiori, A., and Daminelli, G., "Hypersonic Inlet Studies for a Small-Scale Rocket-Based Combined-Cycle Engine", *Journal of Propulsion and Power*, Vol. 23, N. 6, November-December 2007.
- [15] Riva, G., Reggiori, A., and Daminelli, G., "Performance Evaluation of a Ramjet Model in a Pulse Facility at Mach 4.5", *Journal of Propulsion and Power*, Vol. 28, N. 3, May-June 2012.
- [16] Rogers, R.C., Capriotti, D.P., and Guy, R.W., "Experimental Supersonic Combustion Research at NASA Langley", 20th Advanced Measurement and Ground Testing Technology Conference, AIAA Paper 1988-0732, Albuquerque, NM, June 1988.
- [17] Riva, G., Reggiori, A., and Daminelli, G., "A New Pulse Facility for Studies on Rocket.Based Combined-Cycles", *Space Technology*, Vol. 25, N. 2, 2005.
- [18] Heiser, W.H., and Pratt, D.T., "Hypersonic Airbreathing Propulsion", AIAA Education Series, edited by J.S. Przemieniecki, AIAA, Washington DC, 1994.